Molecular Physics, Vol. 104, No. 15, 10 August 2006, 2545–2559

Taylor & Francis
Taylor & Francis Group

Molecular dynamic simulations and global equation of state of square-well fluids with the well-widths from $\lambda = 1.1$ to 2.1

S. B. KISELEV*†, J. F. ELY† and J. R. ELLIOTT JR‡

†Chemical Engineering Department, Colorado School of Mines, Golden, Colorado 80401-1887, USA
‡Chemical Engineering Department, The University of Akron, Akron, OH 44325-3906, USA

(*Received 6 September 2005; accepted 10 October 2005*)

We present the results of extensive new molecular dynamic (MD) simulations in the one-phase region for square well fluids with well widths $\lambda = 1.10$, 1.15, 1.20, 1.25, 1.375, 1.50, 1.75, 1.90, 2.0, and 2.10. These data have been used in developing a crossover equation of state (CR EOS) for square-well fluids with well widths $1.1 \leq \lambda \leq 2.1$. The CR EOS incorporates non-analytic scaling laws in the critical region, and in the limit of low densities yields the exact second and third virial coefficients. Also in the high-temperature region, it reproduces first-order perturbation theory results. The CR EOS was tested against our new MD simulations, and earlier MD and Monte-Carlo (MC) simulations reported by other authors as well. Excellent agreement between calculated values and simulation data for all SW fluids is observed. In combination with the density-functional theory, the CR EOS is also capable of reproducing surface tension simulations with high accuracy. Application of the CR EOS for solid–liquid equilibrium calculations in combination with the Lennard–Jones and Devonshire cell model for the solid phase, is also discussed.

Keywords: Computer simulations; Critical point; Crossover theory; Equation of state; Square-well fluids; Solid–liquid equilibria (SLE); Surface tension; Thermodynamic properties; Vapor–liquid equilibria (VLE)

1. Introduction

One of the fundamental problems in statistical mechanics is to calculate the thermodynamic and interfacial properties of fluids resulting from the interactions between their molecules. The square-well (SW) potential model is the simplest model that incorporates both repulsive and attractive interactions, and has been extensively studied over the last few decades by computer simulations. The interaction energy $u(r)$ between two square-well molecules separated by a distance r is given by

$$u(r) = \begin{cases} \infty & r \leq \sigma \\ -\varepsilon & \sigma < r \leq \lambda\sigma \\ 0 & r > \lambda\sigma \end{cases} \quad (1)$$

where σ is the diameter of the hard-core repulsive interaction, ε is the strength of the attractive interaction, and λ characterizes the width of the attractive interaction. Because of its simplicity, the SW fluid also has been chosen as a reference system in many different theoretical models. However, as we pointed out in our previous work [1], in spite of its importance, no accurate equation of state for the SW fluids with variable well widths has been developed so far. In this paper, we continue the study initiated in our previous work which dealt with $\lambda = 1.5$, 2.0, and 3.0 [1], and present new computer simulations and a new global, crossover equation of state for SW fluids with $1.1 \leq \lambda \leq 2.1$. We proceed as follows: In section 2, we provide the details for our new molecular dynamics simulations. In section 3, we describe a classical Helmholtz free energy for SW fluids, and in section 4 we describe its crossover formulation. A comparison of the new crossover EOS with simulation results for thermodynamic properties and surface tension is presented in section 5. Examples of using the CR EOS for solid–liquid equilibria (SLE) calculations and obtained results are discussed in section 6.

*Corresponding author. Email: skiselev@mines.edu

Molecular Physics
ISSN 0026–8976 print/ISSN 1362–3028 online © 2006 Taylor & Francis
http://www.tandf.co.uk/journals
DOI: 10.1080/00268970600808340

2. Simulations details and results

Molecular dynamics simulations were performed in the microcanonical (NVE) ensemble for 1–3 ns of simulated time. Packing fractions of 0.2 or less were simulated for 3 ns and higher packing fractions were simulated for 1 ns. Estimating the simulated time at each temperature requires assumptions about the mass and energy of the model potentials. The mass was taken as 16 amu and the values of ε/k_B were taken as 312, 288, 266, 247, 194, 146, 106, 73, 73, and 73 K, for $\lambda = 1.1$, 1.15, 1.20, 1.25, 1.375, 1.5, 1.75, 1.9, 2.0, and 2.1, respectively. Simulations for a given potential model along a given isochore were initialized with FCC cells in accordance with the number of atoms (N) simulated in each system. Subsequent simulations along the same isochore were initialized from the final configuration of the preceding simulation with velocities rescaled to reduce the temperature. In our new simulations, the system size was set at 500 molecules in every case, except that additional simulations were performed with 2048 molecules at near critica packing fractions for $\lambda = 1.25$ and 1.375. Packing fractions generally ranged from 0.05 to 0.45 except for the cases of $\lambda = 1.9$ and 2.1, where they stop at $y = 0.30$. The heat capacity of the system was estimated by regressing the values of internal energy U_r with a third-order polynomial and computing the derivative. Note that the fluctuations in compressibility factor were relatively small compared to fluctuations in temperature or internal energy. This happens because higher local temperatures induce higher local pressures. Since the pressure is in the numerator of the compressibility factor and temperature is in the denominator, their fluctuations tend to cancel. Our simulation results along the near critical isochores in SW fluids with $\lambda = 1.25$, 1.375, 1.75, and 2.1 with are given in the appendix. The complete set of the simulation data is available from the authors upon request.

3. Classical free energy

The classical residual Helmholtz free energy of square-well fluids can be represented as a sum of the repulsive hard-sphere contribution A^{HS} and a contribution from the attractive interactions A^{att} [1]

$$A^{res}(T, v) = A^{HS}(T, v) + A^{att}(T, v) \tag{2}$$

where for A^{HS} we use the Carnahan-Starling EOS [2], which accurately represents the thermodynamic properties of HS fluids at high densities and also gives the exact HS second and third virial coefficients in the low-density limit. For the attractive part A^{att} we use the semi-empirical expression proposed in our previous work [1]

$$\frac{A^{att}}{Nk_BT} = -A_0 \ln(1 + A_1\Delta + A_2\Delta^2 + A_3\Delta^3) \tag{3}$$

where N is the number of the particles in the system, k_B is the Boltzmann constant, and $\Delta = \exp[\varepsilon/(k_BT)] - 1$, and the functions A_0, A_1, A_2, and A_3 are given by Pade approximants [1]

$$A_0 = \frac{a_0^{(0)} + a_0^{(2)}y^2 + a_0^{(3)}y^3 + a_0^{(5)}y^5}{1 + b_0^{(2)}y^2} \tag{4}$$

$$A_1 = \frac{1}{A_0}\left[\frac{a_1^{(1)}y}{1 + b_1^{(1)}y + b_1^{(2)}y^2 + b_1^{(3)}y^3}\right] \tag{5}$$

$$A_2 = \frac{a_2^{(2)}y^2 + a_2^{(3)}y^3}{1 + b_2^{(1)}y + b_2^{(2)}y^2 + b_2^{(3)}y^3} \tag{6}$$

$$A_3 = \frac{a_3^{(2)}y^2 + a_3^{(3)}y^3}{1 + b_3^{(1)}y + b_3^{(2)}y^2 + b_3^{(3)}y^3} \tag{7}$$

where $y = \pi\rho\sigma^3/6$ is the packing fraction of the spheres, $\rho = N/V = 1/v$ is the number density of spheres. For the coefficients $a_1^{(1)}$, $b_1^{(1)}$, $a_2^{(2)}$, and $a_3^{(2)}$ we use the same relations as obtained earlier by Kiselev *et al.* [1]

$$a_1^{(1)} = 4(\lambda^3 - 1), \tag{8}$$

$$b_1^{(1)} = \frac{5}{4}\frac{f_1(\lambda)}{(\lambda^3 - 1)}, \tag{9}$$

$$a_2^{(2)} = \frac{1}{a_0^{(0)}}\left[8(\lambda^3 - 1) + \frac{1}{a_0^{(0)}}5f_2(\lambda)\right], \tag{10}$$

$$a_3^{(2)} = \frac{1}{a_0^{(0)}}5f_3(\lambda), \tag{11}$$

where the functions $f_i(\lambda)$ are given by

$$f_1(\lambda) = \begin{cases} 0, & \text{for } \lambda \le 1 \\ \dfrac{1}{5}(\lambda^6 - 18\lambda^4 + 32\lambda^3 - 15), & \text{for } 1 < \lambda \le 2 \\ \dfrac{17}{5}, & \text{for } 2 < \lambda \end{cases} \tag{12}$$

$$f_2(\lambda) = \begin{cases} 0, & \text{for } \lambda \le 1 \\ \frac{2}{5}(\lambda^6 - 18\lambda^4 + 16\lambda^3 - 9\lambda^2 - 8), & \text{for } 1 < \lambda \le 2 \\ \frac{1}{5}(-32\lambda^3 + 18\lambda^2 + 48), & \text{for } 2 < \lambda \end{cases} \tag{13}$$

$$f_3(\lambda) = \begin{cases} 0, & \text{for } \lambda \le 1 \\ \frac{6}{5}(\lambda^2 - 1)^3, & \text{for } 1 < \lambda \le 2 \\ \frac{1}{5}(5\lambda^6 - 32\lambda^3 + 18\lambda^2 + 26), & \text{for } 2 < \lambda. \end{cases} \tag{14}$$

This formulation provides a condition that in the limit of low densities equation (3) exactly reproduces Kihara's analytical expressions [3] for the second and third virial coefficients for the square-well fluids

$$B_2(T) = B_2^{HS}[1 - (\lambda^3 - 1)\Delta] \tag{15}$$

$$B_3(T) = B_3^{HS}[1 - f_1(\lambda)\Delta - f_2(\lambda)\Delta^2 - f_3(\lambda)\Delta^3]. \tag{16}$$

The coefficients $b_1^{(2)}$ and $b_1^{(3)}$ in equation (5) determine the behavior of the residual internal energy U_r in the SW fluids, or, equivalently, the coefficient $A_1' = A_0 A_1$ in the limit $\beta^* = \varepsilon/k_B T \to 0$ [1]. Therefore, the coefficients $b_1^{(2)}$ and $b_1^{(3)}$ can be found from a fit of equations (2)–(5) to the simulation data. In this work, we employ the same expressions for the coefficients $b_1^{(2)}$ and $b_1^{(3)}$ as in our previous work:

$$b_1^{(i)} = b_{1,0}^{(i)} + \sum_{k=1}^{4} b_{1,k}^{(i)} \Delta\lambda^k, \quad i = 2 \text{ and } 3 \tag{17}$$

where the expansion parameter is given by

$$\Delta\lambda = \begin{cases} \lambda - 1.5, & \text{for } \lambda \le 2 \\ \lambda - 3.0, & \text{for } \lambda \ge 2 \end{cases} \tag{18}$$

and the coefficients $b_{1,k}^{(i)}$ for each region are listed in table 1.

Table 1. Coefficients $b_{1,k}^{(i)}$ in equation (17).

Coefficient	$\lambda \le 2$	$\lambda > 2$
$b_{1,0}^{(2)}$	1.5093018500	0.4697011630
$b_{1,1}^{(2)}$	0.9673047240	−4.604133228
$b_{1,2}^{(2)}$	6.3087619550	−26.67612171
$b_{1,3}^{(2)}$	−0.709455318	−43.58375157
$b_{1,4}^{(2)}$	−20.27785515	−19.76736755
$b_{1,0}^{(3)}$	0.5077587980	−0.528853757
$b_{1,1}^{(3)}$	−0.771042541	5.1546638240
$b_{1,2}^{(3)}$	−20.76688587	40.508756730
$b_{1,3}^{(3)}$	−12.04372937	72.750520860
$b_{1,4}^{(3)}$	61.302467810	35.181735840

4. Crossover equation of state

To obtain a crossover formulation of the classical free energy equation (2), we will follow the phenomenological procedure originally developed by Kiselev [4] as generalized recently by Kiselev and Ely [5]. This general approach has been successfully applied for the cubic [4–6, 17, 18], SAFT [19–24], and SAFT-BACK [25] equations of state. Also, in our previous work [1], we used this approach to develop a high accuracy semi-empirical EOS for square-well fluids with $\lambda = 1.5$, 2.0, and 3.0. An advantage of this approach as compared to the more rigorous "microscopic" hierarchical reference theory (HRT) [7–11] and the "globalized" renormalization-group (RG) procedure [12–16] is that the crossover expression for the Helmholtz free energy can be written in a closed analytical form that allows analytical formulation of all derivatives.

In this procedure, we first express the dimensionless Helmholtz free energy $\bar{A}(T, v) = A(T, v)/Nk_B T$ in the form

$$\bar{A}(T, v) = \Delta\bar{A}(\Delta T, \Delta v) + \bar{A}_{bg}(T, v) \tag{19}$$

where the critical part of the Helmholtz free energy is

$$\Delta\bar{A}(\Delta T, \Delta v) = \Delta\bar{A}^{res}(\Delta T, \Delta v) - \Delta\bar{A}^{res}(\Delta T, 0) - \ln(\Delta v + 1) + \Delta v \bar{P}_0(\Delta T) \tag{20}$$

and the background contribution is given by

$$\bar{A}_{bg}(T, v) = -\Delta v \bar{P}_0(T) + \bar{A}_0^{res}(T) + \bar{A}^{id}(T). \tag{21}$$

In equations (19)–(21), $\Delta T = T/T_{0c} - 1$ and $\Delta v = v/v_{0c} - 1$ are dimensionless distances from the classical critical temperature T_{0c} and molar volume v_{0c}, respectively, $\bar{P}_0(T) = P(T, v_{0c})v_{0c}/RT$ is the dimensionless pressure, $\bar{A}_0^{res}(T) = \bar{A}^{res}(T, v_{0c})$ is the dimensionless residual part of the Helmholtz energy along the critical isochore $v = v_{0c}$, and $\bar{A}^{id}(T)$ is the dimensionless temperature-dependent ideal-gas contribution.

In the next step, we replace the classical values of ΔT and Δv in the critical part $\Delta\bar{A}(\Delta T, \Delta v)$ with the renormalized values

$$\bar{\tau} = \tau Y^{-\alpha/2\Delta_1} + (1+\tau)\Delta\tau_c Y^{2(2-\alpha)/3\Delta_1} \tag{22}$$

$$\bar{\varphi} = \varphi Y^{(\gamma-2\beta)/4\Delta_1} + (1+\varphi)\Delta v_c Y^{(2-\alpha)/2\Delta_1} \tag{23}$$

where $\alpha = 0.11$, $\beta = 0.325$, $\gamma = 2-2\beta-\alpha = 1.24$, and $\Delta_1 = 0.51$ are universal non-classical critical exponents [26], $\tau = T/T_c - 1$ is a dimensionless deviation of the temperature from the real critical temperature T_c, $\varphi = v/v_c - 1$ is a dimensionless deviation of the molar volume from the real critical molar volume v_c, $\Delta\tau_c = (T_c - T_{0c})/T_{0c} \ll 1$ and $\Delta v_c = (v_c - v_{0c})/v_{0c} \ll 1$ are dimensionless shifts of the critical temperature and volume, respectively, which can be represented as functions of the Ginzburg number Gi

$$\Delta\tau_c = -\frac{\delta_\tau Gi}{1+Gi}, \quad \Delta v_c = -\frac{\delta_\varphi Gi}{1+Gi} \tag{24}$$

where the coefficients δ_τ and δ_φ are supposed to be system-independent parameters. In our previous study, we found [1], that parameter δ_τ in equation (24) for SW fluid with $\lambda = 1.5$ is extremely small ($\delta_\tau \simeq 10^{-3} \ll 1$) and existing simulation data do not allow us to determine it with a higher accuracy. Therefore, in this work we set $\delta_\tau = 0$ (or $\Delta\tau_c = 0$ in equation (22)), thus implementing a condition $T_c = T_{0c}$. The coefficient δ_φ is considered to be a λ-independent parameter.

In equations (22) and (23), $Y(q)$ denotes a crossover function, for which we use the phenomenological expression used previously [1]

$$Y(q) = \left[\frac{q(1+q)}{1+q+q^2}\right]^{\Delta_1}, \quad q = \frac{r}{Gi}. \tag{25}$$

In this work, the renormalized distance to the critical point r is determined from the recently developed analytical sine-model (ANS) equation [27]

$$r = \frac{4((b/m_0)|\varphi|)^{1/\beta} + 2\tau + \sqrt{[4((b/m_0)|\varphi|)^{1/\beta} + 2\tau]^2 + 12\tau^2}}{6}, \tag{26}$$

where the coefficients m_0 and v_1 are the system-dependent parameters, and $b^2 = (\gamma-2\beta)/[\gamma(1-2\beta)] \cong 1.359$ is a universal linear-model parameter [28, 29]. Since the ANS model does not require a numerical solution of a transcendental equation for the parameter q, this modification makes calculation of all derivatives of the crossover function $Y(q)$ with respect to the temperature and density much simpler than in the EOS developed earlier [1]. Otherwise, the crossover models presented here and in our previous work [1] are physically equivalent.

In order to complete the transformation, one needs to add in equation (19) the kernel term

$$K(\tau) = \frac{1}{2}a_{20}\left(\frac{\tau}{1+\tau}\right)^2 (Y^{-\alpha/\Delta_1} - 1) \tag{27}$$

which provides the correct scaling behavior of the isochoric heat capacity $C_v = -T(\partial^2 A/\partial T^2)_{v=v_c} \propto a_{20}|\tau|^{-\alpha}$ along the critical isochore $v = v_c$ asymptotically close to the critical point at $|\tau| \ll Gi$ [1]. Finally, the crossover expression for the Helmholtz free energy can be written in the form [1]

$$\bar{A}(T,v) = \bar{A}^{res}(\bar{\tau},\bar{\varphi}) - \bar{A}^{res}(\bar{\tau},0) - \ln(\bar{\varphi}+1) + \bar{\varphi}\bar{P}_0(\bar{\tau},0) - \Delta v\bar{P}_0(T) + \bar{A}_0^{res}(T) + \bar{A}^{id}(T) - K(\tau). \tag{28}$$

Equations (19)–(28), together with equations (2)–(7) for the classical Helmholtz free energy, completely determine the crossover formulation for the Helmholtz free-energy in SW fluids. The crossover equations for the pressure $P(T,v) = -(\partial A/\partial v)_T$ and the internal energy $U(T,v) = A + TS = A + T(\partial A/\partial T)_v$ can be obtained from the crossover expression (28) by differentiation with respect to volume and temperature, respectively.

5. Comparisons with simulation data

5.1. *Thermodynamic properties*

In order to develop a crossover EOS for the SW fluid of interest one needs to specify the original classical parameters $a_j^{(i)}$ and $b_j^{(i)}$ in equations (4)–(7), as well the crossover parameters a_{20}, Gi, m_0 and v_1 in equations (24)–(28). In this work, in developing a crossover EOS for SW fluids with varying well width (similar to the parameters $b_1^{(i)} (i = 2, 3)$) the classical parameters $a_0^{(0)}$, $a_0^{(2)}$, $a_0^{(3)}$, $a_0^{(5)}$, $a_2^{(3)}$, $a_3^{(3)}$, $b_0^{(2)}$, $b_2^{(2)}$, and $b_2^{(3)}$ (denoted as c_m) have been expressed by truncated Taylor expansions

$$c_m(\lambda) = c_{m,0} + \sum_{k=1}^{4} c_{m,k}\Delta\lambda^k \tag{29}$$

Table 2. Coefficients $c_{m,n}$ in equation (29) for the classical parameters $a_i^{(j)}$ and $b_i^{(j)}$ in the attractive part of the Helmholtz free energy equation (3) for the square-well fluids with $1.1 \le \lambda \le 2.1$.

c_m	$c_{m,0}$	$c_{m,1}$	$c_{m,2}$	$c_{m,3}$	$c_{m,4}$
$a_0^{(0)}$	1.433616E+00	1.708540E+00	−9.488607E-01	5.980393E-02	0
$a_0^{(2)}$	−4.378564E+00	−2.577181E+01	3.511119E+01	1.983882E+02	0
$a_0^{(3)}$	2.394942E+01	1.411165E+02	3.864338E+01	−4.340290E+02	2.445365E+02
$a_0^{(5)}$	−5.313752E+01	−2.659828E+02	9.110143E+00	1.282316E+03	−8.151838E+01
$a_2^{(3)}$	2.408875E+01	1.202626E+02	1.407579E+02	−1.106967E+01	0
$a_3^{(3)}$	−2.909988E-01	−1.675850E+01	−6.948178E+01	−6.297907E+01	0
$b_0^{(2)}$	−6.339525E-01	9.255354E+00	2.411173E+01	3.283827E+01	0
$b_2^{(2)}$	−6.101644E+00	−4.546820E+01	5.103082E+01	6.825992E+01	−7.290768E+00
$b_2^{(3)}$	2.477978E+01	1.362488E+02	−9.406375E+01	−1.382791E+02	−1.022288E+02

where (unlike equation (18)) $\Delta\lambda = \lambda - 1.375$. The coefficient v_1 in equation (26) appears to be small and statistically irrelevant ($v_1 = 7.7 \times 10^{-8} \pm 2.2 \times 10^{-6}$). For all SW fluids we have set $\delta_\varphi = 0.2$, while the amplitude a_{20} in the kernel term equation (27), the inverse Ginzburg number $g = Gi^{-1}$, and coefficients m_0, designed as k_i, have been expressed as simple linear functions of $\Delta\lambda$

$$k_i = k_{i,0} + k_{i,1}\Delta\lambda. \tag{30}$$

The coefficients $c_{m,n}$ and $k_{i,j}$ in equations (29) and (30) have been found from a fit of equation (28) to the new MD results for SW fluids obtained in this work, as well the molecular dynamic (MD) and Monte-Carlo (MC) simulations results obtained earlier [1, 31]. The numerical values of the coefficients $c_{m,n}$ and $k_{i,j}$ ($j = 0, 1$) for fluids with $1.1 \le \lambda \le 2.1$ are listed in tables 2 and 3. The results of our calculations for various thermodynamic properties are shown in figures 1–5. As one can see, the only systematic deviations between the MD simulation $U_r - \beta^*$ and $Z - \beta^*$ data in the case where $\lambda = 1.75$ at $y > 0.45$ (or $y > 3y_c$) and $\beta^* < 1.0$ (or $T_c^* < 0.556$). As discussed below, one of the possible explanations for these deviations is that these points actually belong to the solid, rather than liquid phase. Otherwise, excellent agreement between simulation data and the crossover EOS for both the one and two-phase regions is observed for all SW fluids with $1.25 \le \lambda \le 2.1$. In the entire density and temperature regions shown in figures 1–3, the crossover EOS reproduces the compressibility factor with an average absolute deviation (AAD) of about 1.25% and residual internal energy with an AAD of about 0.85%.

As we mentioned above, the kernel term $K(\tau)$ was introduced in equation (28) to provide a correct asymptotic scaling behavior of the isochoric heat capacity in the critical region. In figures 6 and 7, we show comparisons between the MD and MC C_V-data for the SW fluids with $\lambda = 1.5$ and 2.0 and the values of the isochoric heat capacity calculated with the CR EOS. For the SW fluid with $\lambda = 1.5$ and $N = 2048$ (the biggest system) excellent agreement is observed between the MC results and the predicted values over the entire range $0 < \beta^* < 0.8$ (or $T^* \ge 1.025T_c^*$). For the SW fluid with $\lambda = 2.0$, only qualitative agreement between the MD simulations and calculated values is observed. As we discussed in our previous work [1], asymptotically close to the critical point the MD simulations are not very reliable, while the CR EOS at $|\tau| \to 0$ does reproduce the theoretically well established scaling behavior $C_V \propto |\tau|^{-\alpha}$.

Table 3. Coefficients $k_{i,j}$ in equation (30) for the parameters a_{20}, g, m_0, and δ_φ for the square-well fluids with $1.1 \le \lambda \le 2.1$.

k_i	$k_{i,0}$	$k_{i,1}$
a_{20}	2.875229E+00	−9.327260E-01
g	1.395759E+00	6.680527E-01
m_0	8.731365E-01	−2.207693E-03
δ_φ	2.0E-01	0

Because of finite size effects, the determination of the critical parameters of SW from the VLE MD and MC simulations is a challenging task [32, 33]. Therefore, it is interesting to compare the critical parameters obtained for SW fluids with $1.1 \le \lambda \le 2.1$ by different methods. The values of the critical parameters T_c^*, y_c, and P_c^*, the critical compressibility $Z_c = P_c/R\rho_c T_c$, and acentric factor $\omega = -\log(P_S/P_c)|_{T=0.7T_c} - 1$ (where P_S is a vapor pressure) as functions of the well-width λ calculated with the CR EOS and obtained by other

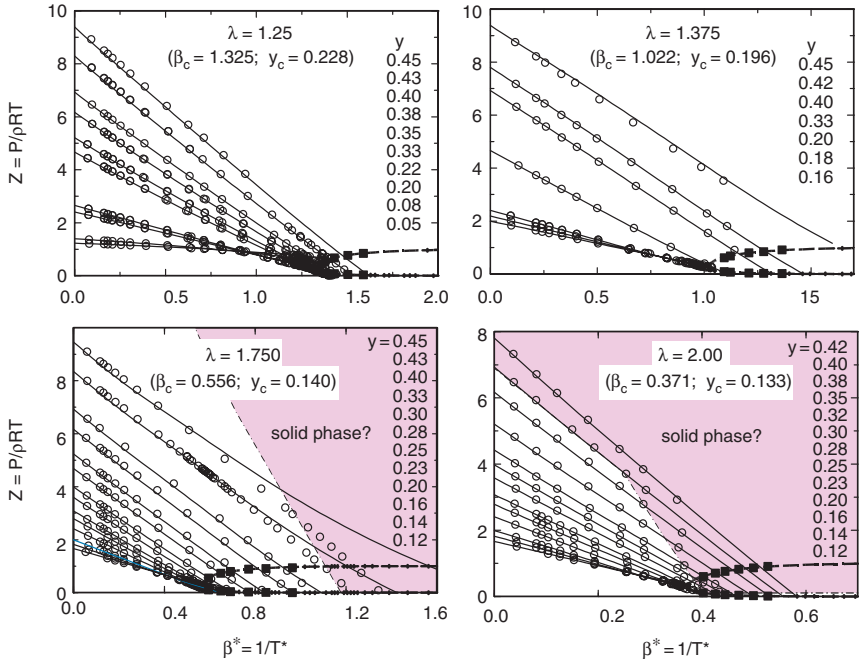

Figure 1. Compressibility factor Z along various isochores as functions of the inverse temperature $\beta^* = 1/T^*$ or square-well fluids with $\lambda = 1.25$, 1.375, 1.75, 2.0. The symbols correspond to the molecular dynamics results and the lines represent the values calculated with the crossover EOS.

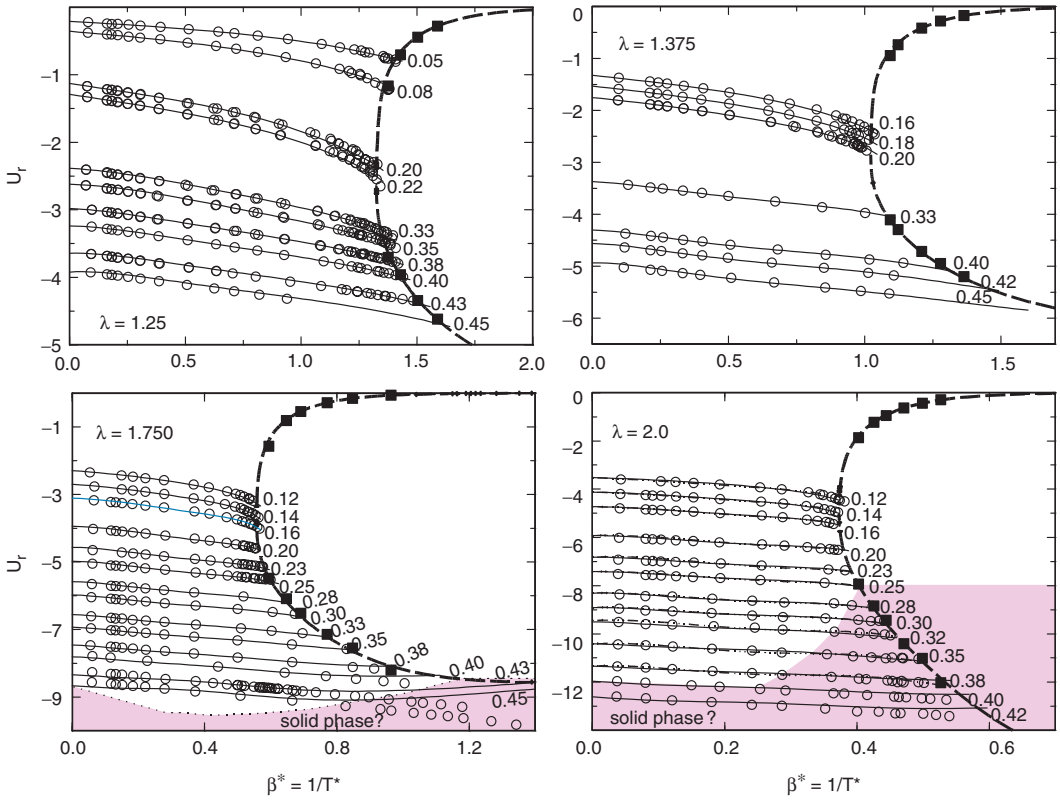

Figure 2. Residual internal energy U_r along various isochores as functions of the inverse temperature $\beta^* = 1/T^*$ for square-well fluids with $\lambda = 1.25$, 1.375, 1.75, and 2.0. The symbols correspond to the molecular dynamic results and the curves represent the values calculated with the crossover EOS.

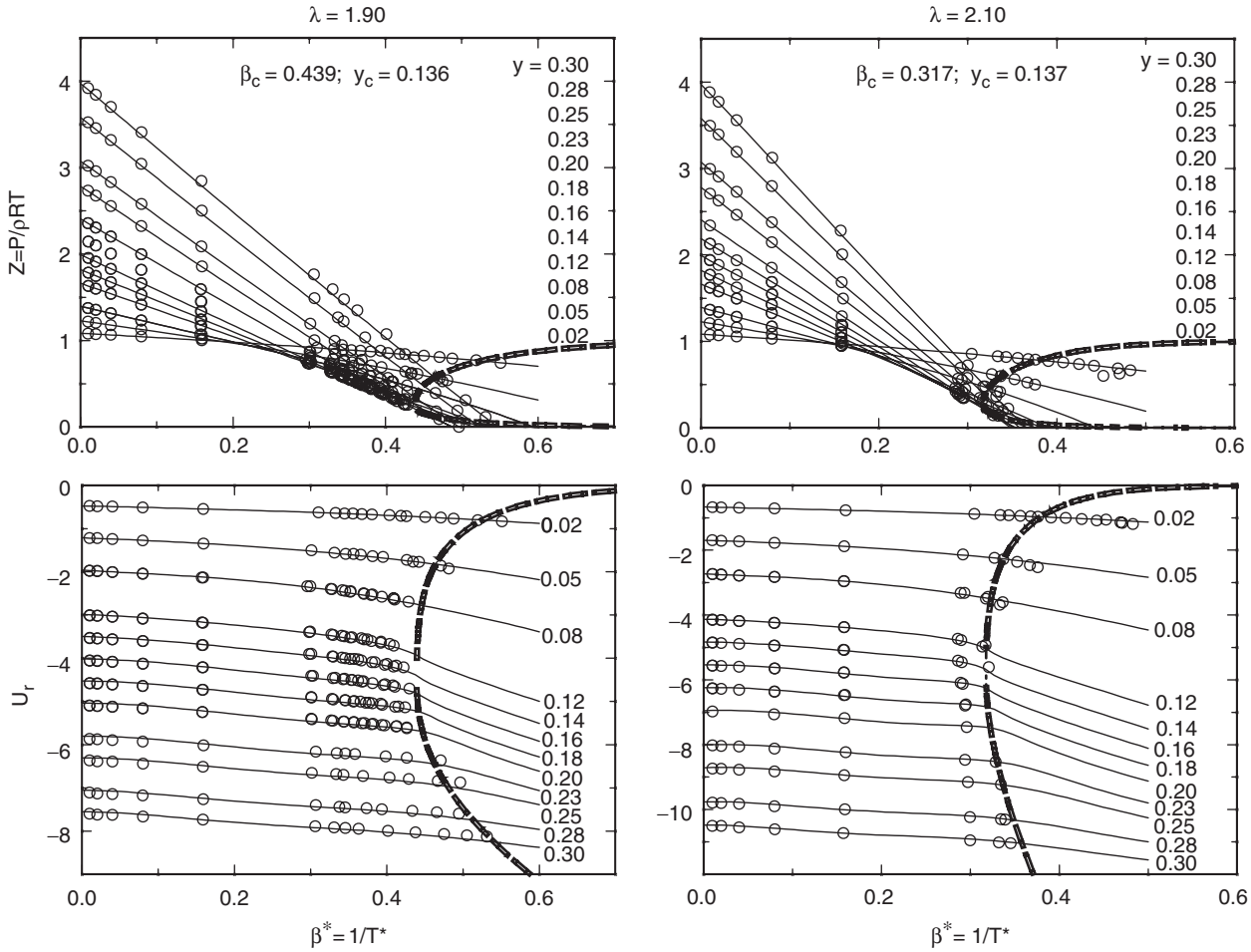

Figure 3. Compressibility factor Z (top) and residual internal energy U_r (bottom) along various isochors as functions of the inverse temperature $\beta^* = 1/T^*$ for square-well fluids with $\lambda = 1.90$ (left) and 2.10 (right). The symbols correspond to the molecular dynamic results and the lines represent the values calculated with the crossover EOS.

methods are shown in figures 8 and 9. The little "humps" observed at $\lambda \approx 1.4$ for P_c and at $\lambda \approx 1.6$ for Z_c are the result of the chosen parameterization and, in principle, can be smoothed by adding the extra terms in equations (29) and (30). However, even in the present form a reasonably good agreement between the CR EOS predictions, simulation results, and values obtained by other authors is observed. The plus symbols in figure 9 correspond to the values of Z_c in some real fluids considered earlier in our previous works [5, 34]. As one can see, the real fluids in general do not match a $Z_c - \omega$ path obtained for the SW fluids. Except for the noble gases argon ($Z_c = 0.292$; $\omega = -0.004$) and krypton ($Z_c = 0.288$; $\omega = -0.002$), and also light and heavy water ($Z_c \cong 0.229$; $\omega \cong 0.344$), experimental values lie far from the calculated curve $Z_c(\omega)$. For krypton and water, the deviations of the saturated liquid densities calculated with the CR EOS from experimental data are very large (see figure 10). A better matching the binodal and vapor pressure curve of krypton gives a value of $\lambda = 1.750$ (see dotted-dashed lines in figure 10), but with smaller $Z_c = 0.262$ compared to the experimental value of 0.288. This means that SW monomers may not be a good choice as a reference system in the thermodynamic perturbation theory (TPT) equation of state for real fluids.

5.2. *Surface tension*

The crossover EOS not only yields an excellent description of one-phase thermodynamic and VLE properties for all SW fluids with $1.25 \leq \lambda \leq 2.1$, but it can be further extended into the metastable and unstable regions, thus reproducing the continuous vdW loops.

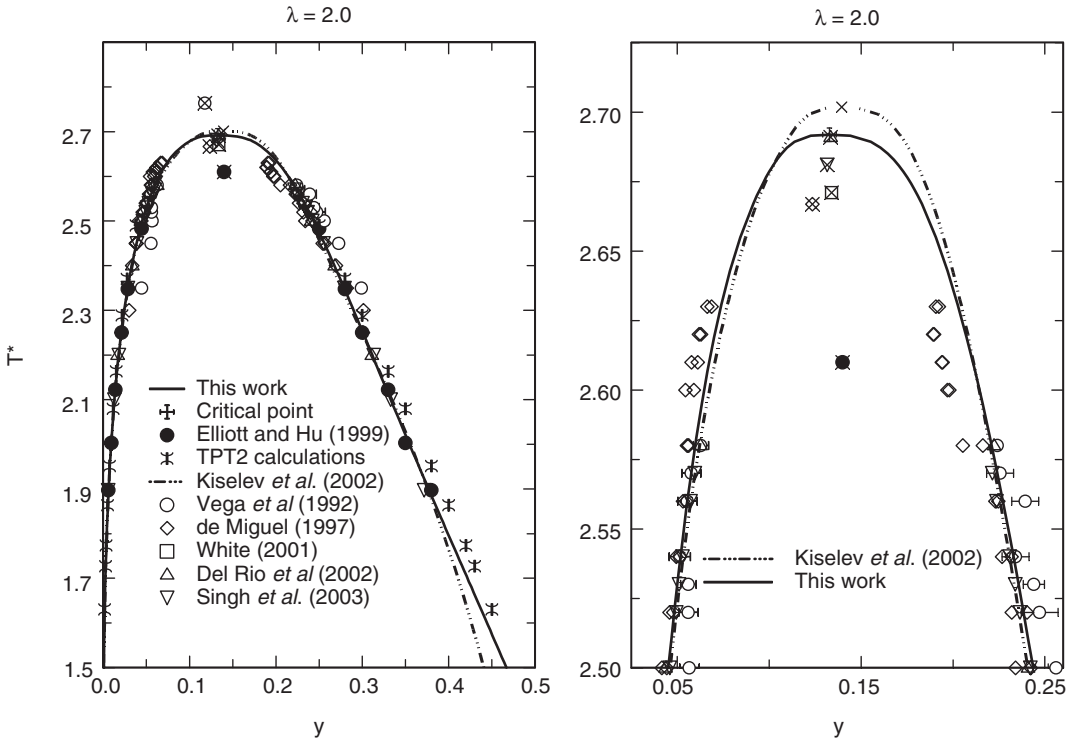

Figure 4. Coexistence curve of the square-well fluid with $\lambda = 2.0$. The symbols correspond to the computer simulation results [31, 35, 44–46], the second-order thermodynamic perturbation theory TPT2 (ants), and the global renormalization method calculations [16] (empty squares). The crosses mark the critical point, and the curves represent the values calculated with the crossover EOS (solid curves) and with the CR EOS-02 [1] (dotted-dashed curves).

This allows us to apply it, in combination with the density-functional theory (DFT), to surface tension calculations. The crossover DFT formulation for the surface tension on the planar liquid-vapor interface is given by [5]

$$\sigma = c_0^{1/2} \int_{\rho_V}^{\rho_L} [\Delta \hat{A}(\rho)]^{1/2} d\rho \tag{31}$$

where $\Delta \hat{A}(\rho) = \rho RT \Delta \bar{A}(T, \rho) = \hat{A}_b(T, \rho) - \rho \mu(T, \rho_{V,L})$ is an excess part of the Helmholtz free energy density calculated with the crossover EOS (28), and $\mu(T, \rho_{V,L}) = (\partial \rho A / \partial \rho)_T$ is a chemical potential of the bulk fluid along the saturated curve $\rho = \rho_{V,L}(T)$. The temperature dependence appears in the crossover DFT model (31) through the excess free-energy density $\Delta \hat{A}(\rho)$ and the parameter c_0. In our previous study we showed [5] that for simple fluids, a good estimate for this parameter is $c_0 \cong k_B T_c \rho_c^{1/3}$. Following that study, for square-well fluids we adopt the temperature-independent parameter c_0 in the form

$$c_0 = (1 - \kappa_0)^2 k_B T_c \rho_c^{1/3}, \tag{32}$$

where parameter $\kappa_0 < 1$. We found, that for the SW fluids with $1.25 < \lambda < 2.1$ a good approximation for this parameter is

$$\kappa_0 = 0.53 - 0.2\lambda \tag{33}$$

The results of our calculations in comparison with the MC simulation results for the surface tension in square-well fluids with $\lambda = 1.5$, 1.75 and 2.0 obtained by Singh *et al.* [35] are shown in figure 11. Again, excellent agreement between calculated values and simulation data for all SW fluids is observed. Except for a few data points where $|\tau| < 0.05$, the CR EOS/DFT model reproduces the MC simulation results for the surface tension [35] with an AAD of about 1–2%.

6. Discussion

SW systems capture the essential features of real materials while remaining simple enough to treat using analytic and simulation methods. However, most

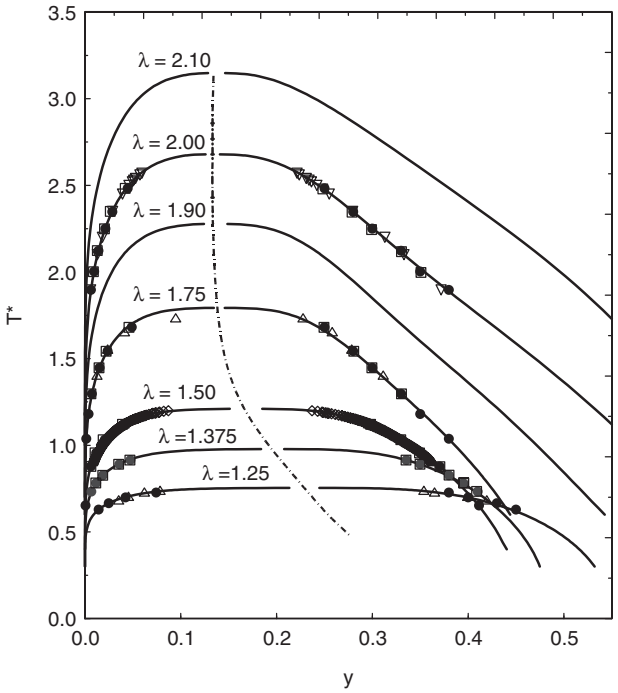

Figure 5. Coexistence curve of the square-well fluids with $\lambda = 1.25 - 2.1$. The symbols correspond to the simulation results by Elliott and Hu [31] (filled circles), by Singh *et al*. [35] (triangles down), by del Rio *et al*. [46] (triangles up), by Orkoulas and Panagiotopoulos [33] (dimonds), and the global renormalization method calculations [16] (empty squares). The curves represent the values of the critical packing fraction (dotted-dashed curves) and VLE data (solid curves) calculated with the crossover EOS.

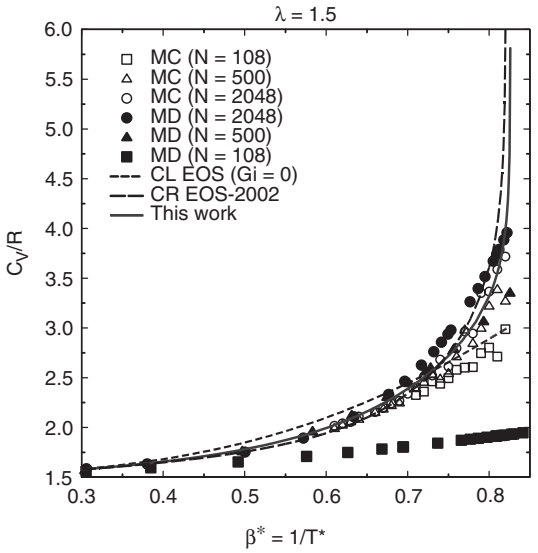

Figure 6. Isochoric heat capacity along the near-critical isochore $y = 0.16$ for the square-well fluid with $\lambda = 1.5$. The symbols, dashed, and dashed-dotted curves correspond to the values obtained by Kiselev *et al*. [1], and the solid curve calculated with the crossover EOS.

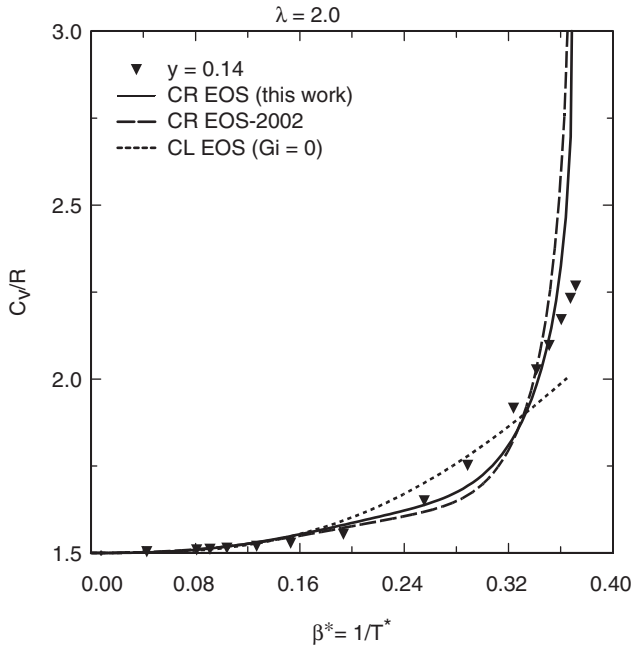

Figure 7. Isochoric heat capacity along the near-critical isochore $y = 0.14$ for the square-well fluid with $\lambda = 2.0$. The symbols, dashed, and dashed-dotted curves correspond to the values obtained by Kiselev *et al*. [1], and the solid curve calculated with the crossover EOS.

previous studies of SW fluids have been concentrated on the one-phase *PVT* and VLE properties, and no systematic study of the solid–liquid equilibrium (SLE) in SW fluids has been performed thus far. Since SLE calculations require an accurate EOS for representation of the liquid densities, $\rho(P, T)$, in a wide interval pressures and temperatures, a self-consistent Helmholtz energy model should be used for these calculations. In this work, we presented new extensive MD simulations and developed a global equations of state for SW fluids with $1.1 \leq \lambda \leq 2.1$, which far from the critical point, at $|\tau| \geq 0.05$, represents all reliable MD and MC simulations with a high accuracy and in the critical region, at $|\tau| \to 0$, reproduces all theoretically well-established scaling laws. Therefore, it is also interesting to apply this EOS to SLE calculations.

Our preliminary results for the global phase diagram for SW fluids with $\lambda = 1.5$, 2.0, and $\lambda = 1.75$ calculated with the CR EOS and Lennard–Jones and Devonshire (LJD) cell model [36] are shown in figures 12 and 13, respectively. The squares in figures 12 and 13 represent the SLE densities calculated with the LJD cell model [36] for both, liquid and solid phases, while the curves correspond to the values calculated with the crossover EOS for the liquid phase and the LJD cell model for the solid phase. Since the zero level of the Helmholtz

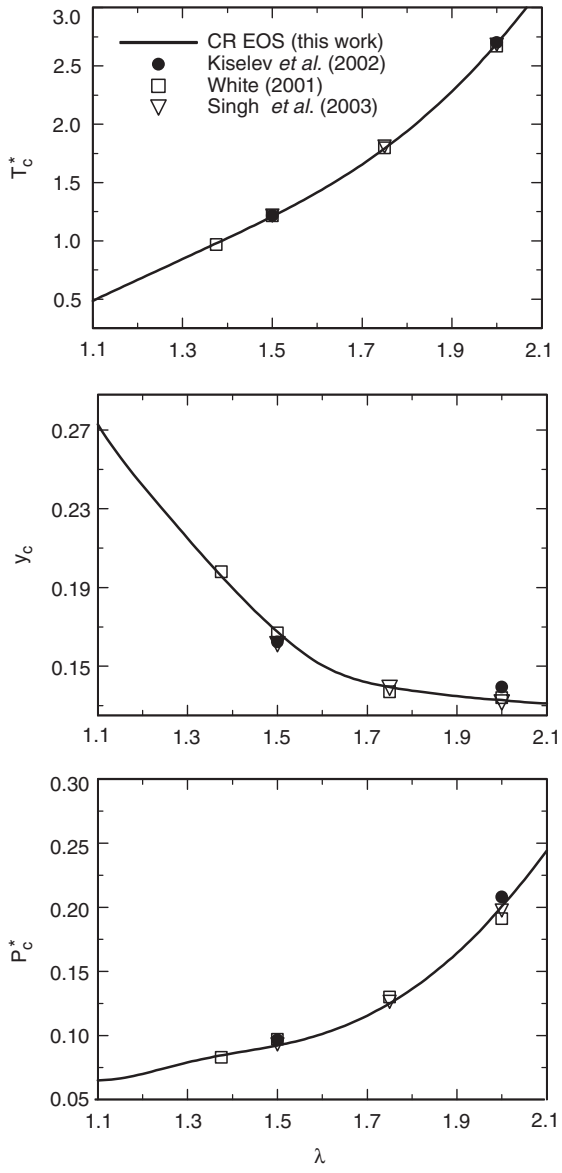

Figure 8. Critical parameters T_c^*, y_c, and P_c^* of square-well fluids as functions of the well-width λ. The curves represent the values calculated with the crossover EOS and the symbols correspond to the values obtained earlier by other authors [1, 16, 35].

free-energy in the crossover model, f_o^{CR}, and in the LJD cell model [36], f_o^{LJD}, can be chosen arbitrarily and in general do not coincide, the calculations have been performed with a zero parameter $f_0 = f_o^{LJD} - f_o^{CR}$ and $f_0 = 1.76$. As one can see, in the latter case the CR EOS/LJD model reproduces the MD simulations for SW fluid with $\lambda = 1.5$ reported by Young and Alder [37], but with a stable hexagonal close-packed (hcp) phase up to $T^* = 2.5$. No stable face-centered cubic (fcc) phase that was predicted by Young and Alder [37] at $T^* > 1.2$ is observed.

For the SW fluid with $\lambda = 1.75$, the stable hcp phase is observed only where $T^* > 2.4$, and at lower temperatures the stable body-centered cubic (bcc) phase is observed. The solid state region, which corresponds to our results presented in figure 12, is marked in figures 1 and 2 by shaded area. In accordance with these calculations, all MD simulations for SW fluid with $\lambda = 1.75$ with $y > 0.45$ and $\beta^* < 1.0$, as we pointed it out in the previous section, do belong to the solid phase region.

For the SW fluid with $\lambda = 2.0$, the SLE calculations are inconsistent with MD VLE simulation data reported by Elliott and Hu [38]. In both cases, with zero and non-zero f_0, the CREOS/LJD model predicts a triple point temperature ($T_{tr} = 2.5$ and 2.25, respectively), which is higher than a minimum temperature reported in Ref. [38] (see also shaded area in figures 2 and 3). For SW fluids with $\lambda < 1.5$, the discrepancy between MD VLE simulations and CR EOS/LJD model SLE calculations is even more dramatic. The global phase diagram for SW fluid with $\lambda = 1.375$ calculated with the CR EOS/LJD model with $f_0 = 0$ is shown in figure 14. As one can see, according to these calculations, no liquid states exist in this system. A similar situation arises for $\lambda = 1.25$.

We should note that in principle this result is not fully unexpected. Similar results have been obtained earlier for the short-range attractive Yukawa [39] and empirical Girifalco [40] potentials. However, for SW fluids these phase diagrams have not been observed before. We are not aware of any representative MD or MC simulations, or any theoretically self consistent model for the VLE and SLE properties in this system, and cannot say for sure what causes this discrepancy. If it is an artifact of the discontinuous potential in the MD simulations [37, 38], or a result of an ''illegal'' combination of the CR EOS with the LJD cell model [36]. Note, however, that the MD simulations for $\lambda < 1.5$ appear to be unperturbed by the possible presence of a more stable solid phase, making it possible to characterize the global VLE for small λ. We may only speculate that these consistent VLE result from the entire VLE binodal being inside the metastable region (as opposed to being crossed at $y = 0.45$ for $\lambda = 1.75$), or from a kinetic resistance that develops for small λ. In order to answer these questions, a more detailed theoretical study and new computer simulations for SW fluids with $\lambda < 1.5$ are needed. It is also interesting to compare the present CREOS/LJD predictions for SW fluids with the SLE phase diagram calculated with the CR EOS for liquid and thermodynamic perturbation theory [41–43] for the solid phase. Work in this direction is now in progress, and the results will be reported in future publications.

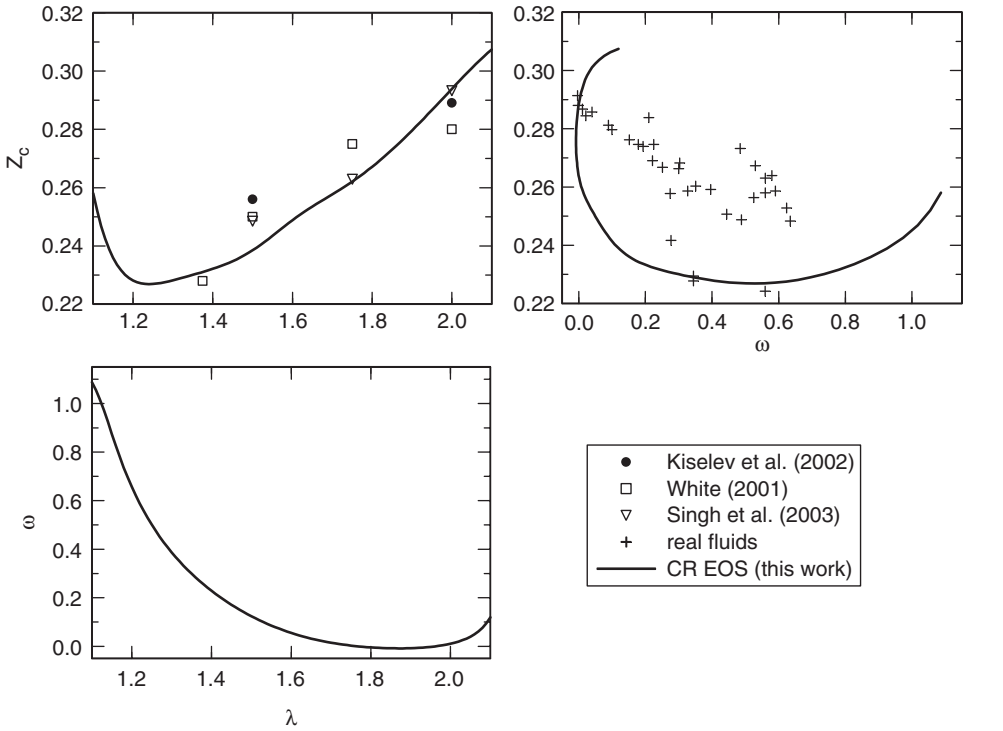

Figure 9. Critical compressibility factor Z_c (top) and the acentric factor ω (bottom) as functions of the well-width λ. The curves represent the values calculated with the crossover EOS, the symbols correspond to the values obtained earlier by other authors [1, 16, 35], and the plusses correspond to the selected experimental values for pure fluids [5, 34].

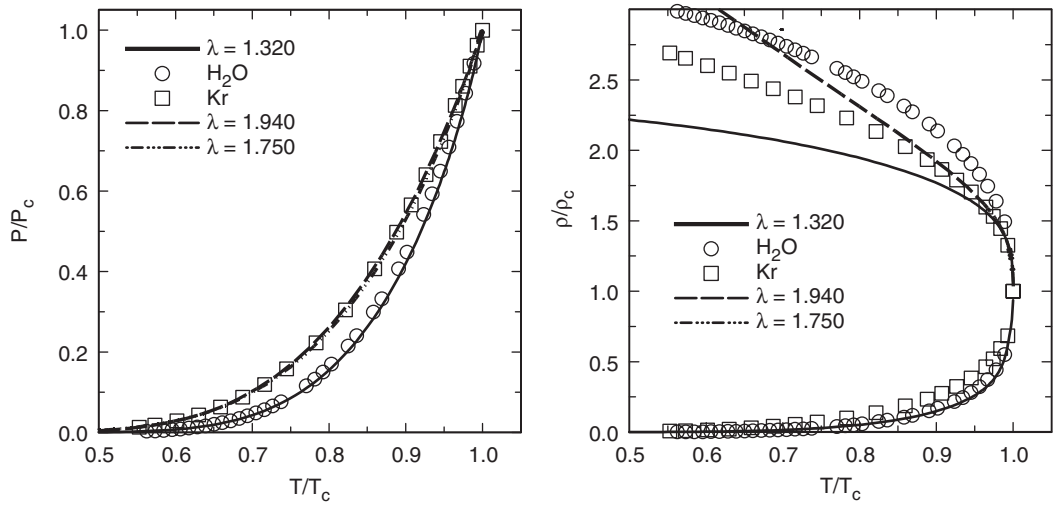

Figure 10. The saturated pressure (top) and saturated density (bottom) data for water [47] and krypton [48] (symbols) with predictions of the crossover EOS (curves).

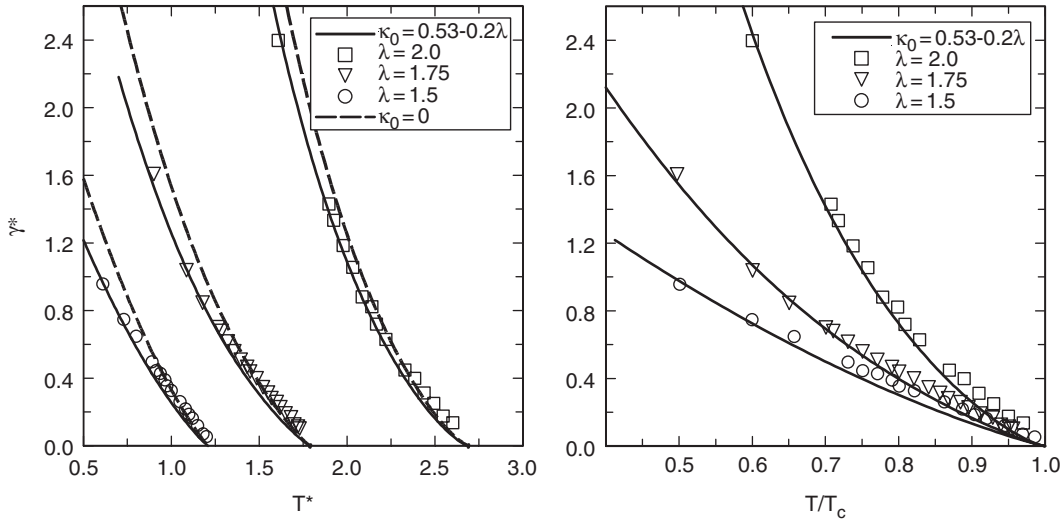

Figure 11. The surface tension Monte-Carlo simulation results for square-well fluids with $\lambda = 1.5$, 1.75, and 2.0 (symbols) with predictions of the CR EOS-DFT model with $\kappa_0 = 0$ (dashed curve) and $\kappa_0 = \kappa_0(\lambda)$ (solid curves).

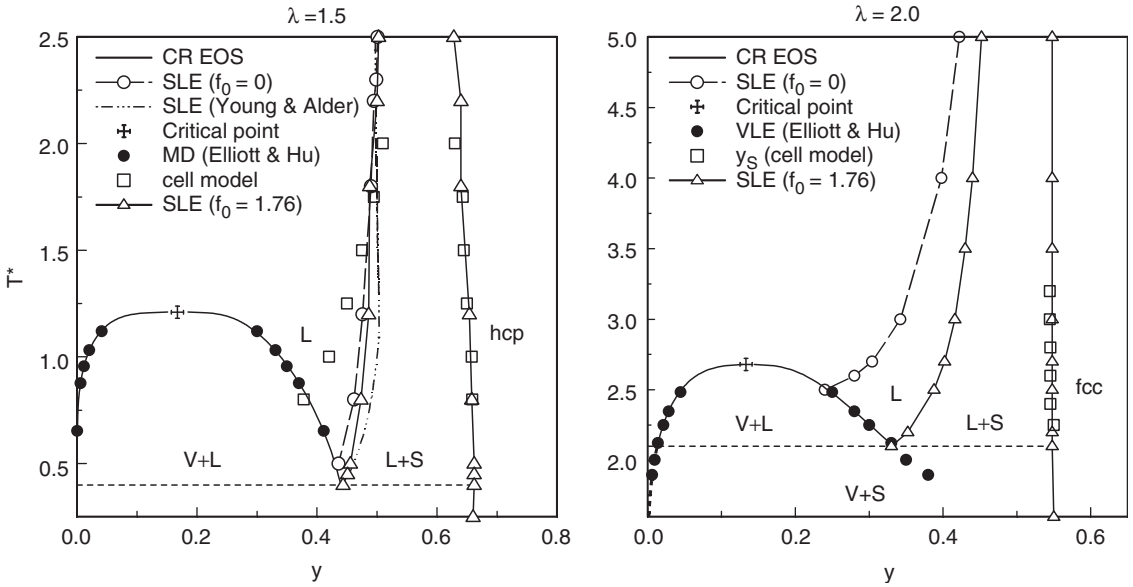

Figure 12. Phase diagram for SW fluids with $\lambda = 1.5$ (left) and $\lambda = 2.0$ (right). The solid, solid with triangles, and dashed with empty circles curves represent the CR EOS (liquid phase) + cell model (solid phase) calculations, the dotted-dashed curves correspond to the MD SLE simulation results for the SW fluid with $\lambda = 1.5$ [37], the squares represent the cell-model predictions, and the filled symbols represent the MD VLE simulations [38].

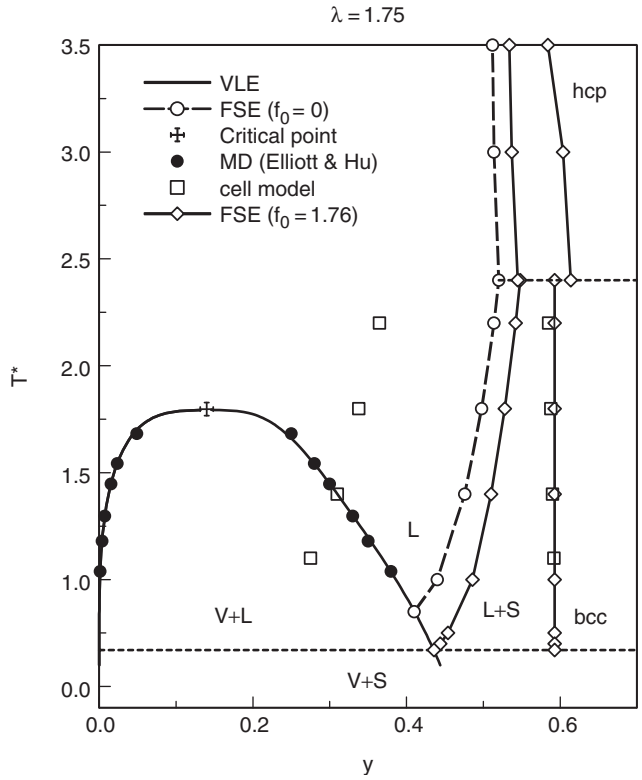

Figure 13. Phase diagram of the square-well fluid with λ = 1.75. The VLE curves calculated with the crossover EOS, the squares represent the cell-model predictions, and the SLE curves represent the CR EOS (liquid phase) + cell model (solid phase) calculations.

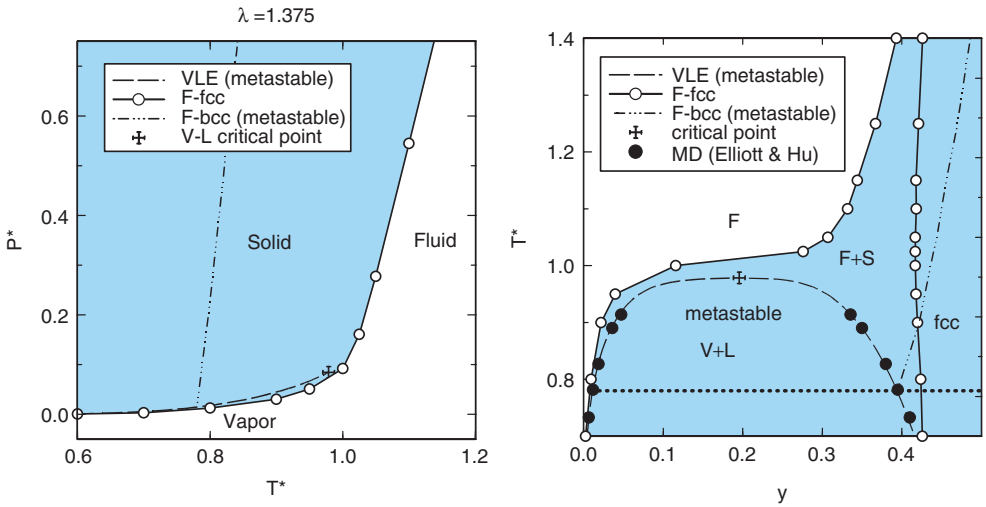

Figure 14. The *P-T* (top) and *P-V* phase diagram of the square-well fluid with λ = 1.375. The VLE (dashed curves) calculated with the crossover EOS, the solid curves with empty circles curves represent the CR EOS (liquid phase) + cell model (solid phase) calculations, and the filled symbols represent the MD VLE simulations [38].

Acknowledgements

The research in the Colorado School of Mines was supported by the US Department of Energy, Office of Basic Energy Sciences, under Grant No. DE-FG03-95ER14568. JRE acknowledges support from the NIST-CSTL group, Boulder, CO for two summer visits, and from ChemStations, Inc. Houston, TX, for support of the SPEADMD project.

Appendix. MD simulation results along the near critical isochores in SW fluids with λ = 1.25, 1.375, 1.75, and 2.1.

$\lambda = 1.25$	$N = 2048$	$y = 0.220$	$\lambda = 1.75$	$N = 500$	$y = 0.1404$
0.07566	−1.33161	2.52244	0.06745	−2.76847	1.62580
0.16165	−1.37867	2.36487	0.15067	−2.85093	1.38534
0.18209	−1.39178	2.32618	0.18356	−2.88530	1.29127
0.20865	−1.40059	2.27858	0.22201	−2.92247	1.18198
0.25165	−1.43014	2.19688	0.27898	−2.98893	1.01640
0.30502	−1.46234	2.09808	0.36777	−3.11244	0.76577
0.38569	−1.51042	1.94552	0.41460	−3.18129	0.63531
0.50969	−1.58967	1.71349	0.46185	−3.28838	0.50229
0.62433	−1.66510	1.49901	0.49259	−3.36049	0.42519
0.71019	−1.73070	1.33834	0.50979	−3.40522	0.37908
0.80339	−1.80349	1.16495	0.52076	−3.45248	0.34479
0.91000	−1.89582	0.96676	0.53066	−3.50468	0.32354
1.06205	−2.05193	0.68774	0.53546	−3.52722	0.31130
1.12334	−2.13223	0.57105	0.54521	−3.55567	0.28672
1.17970	−2.21446	0.47430	0.55468	−3.61610	0.26524
1.20991	−2.25985	0.41961	0.56335	−3.68485	0.24701
1.23509	−2.30836	0.37824	0.57297	−3.78259	0.22247
1.25960	−2.36193	0.33387	0.58143	−3.87927	0.20354
1.27489	−2.39404	0.31080	0.59752	−4.02653	0.16434
1.29709	−2.44815	0.26808	0.60368	−4.19475	0.15264
1.31036	−2.49998	0.25071	0.61236	−4.38069	0.13758
1.32655	−2.54900	0.22092	0.62908	−4.55666	0.11008
1.34253	−2.65238	0.19901	0.64320	−4.77286	0.08736
1.36270	−2.71788	0.17429	0.66081	−4.97784	0.05877
1.37879	−2.83690	0.14649	0.68484	−5.23353	0.02813
1.40075	−2.97523	0.12743			
1.43067	−3.15609	0.10134			
1.46278	−3.36850	0.06367			
1.50936	−3.59822	0.02950			
$\lambda = 1.375$	$N = 500$	$y = 0.200$	$\lambda = 2.10$	$N = 2048$	$y = 0.140$
0.09541	−1.80410	2.20384	0.01008	−4.85378	1.77053
0.21311	−1.88171	1.93916	0.07960	−4.94890	1.42685
0.24336	−1.90215	1.87227	0.15814	−5.07729	1.03991
0.27585	−1.92325	1.79796	0.29050	−5.45521	0.40187
0.33543	−1.96007	1.66451	0.01003	−5.56182	1.93851
0.40510	−2.01408	1.51168	0.07967	−5.65503	1.54581
0.50542	−2.08835	1.29113	0.15807	−5.77663	1.10393
0.65465	−2.22429	0.96704	0.29141	−6.12422	0.37344
0.73795	−2.30162	0.79145	0.00998	−6.26725	2.12734
0.82536	−2.40838	0.60515	0.07964	−6.36340	1.68516
0.86999	−2.48641	0.50334	0.15788	−6.47363	1.19000
0.91808	−2.56277	0.40710	0.29407	−6.79245	0.34878
0.96546	−2.62524	0.32853	0.00994	−6.97156	2.33920
0.97272	−2.66085	0.30681	0.07943	−7.06190	1.85011
0.97689	−2.66122	0.30111	0.15866	−7.18088	1.29238
0.99207	−2.70889	0.27210	0.29595	−7.45764	0.34403

References

[1] S. B. Kiselev, J. F. Ely, L. Lue, and J. R. Elliott Jr, Fluid Phase Equilib. **200,** 121 (2002).
[2] N. F. Carnahan and K. E. Starling, J. Chem. Phys. **51,** 635 (1969).
[3] T. Kihara, Rev. Mod. Phys. **25,** 831 (1953).
[4] S. B. Kiselev, Fluid Phase Equilib. **147,** 7 (1998).
[5] S. B. Kiselev and J. F. Ely, J. Chem. Phys. **119,** 8645 (2003).
[6] S. B. Kiselev and D. G. Friend, Fluid Phase Equilib. **162,** 51 (1999).
[7] A. Parola and L. Reatto, Phys. Rev. Lett. **53,** 2417 (1984).
[8] A. Parola and L. Reatto, Phys. Rev. A **31,** 3309 (1985).
[9] A. Parola, A. Meroni, and L. Reatto, Int. J. Thermophys. **10,** 345 (1989).
[10] M. Tau, A. Parola, D. Pini, and L. Reatto, Phys. Rev. E **52,** 2644 (1995).
[11] L. Reatto and A. Parola, J. Phys.: Condens. Matter **8,** 9221 (1996).
[12] J. A. White and S. Zhang, J. Chem. Phys. **103,** 1922 (1990).
[13] J. A. White and S. Zhang, J. Chem. Phys. **99,** 2012 (1993).
[14] J. A. White, J. Chem. Phys. **111,** 9352 (1999).
[15] J. A. White, J. Chem. Phys. **112,** 3236 (2000).
[16] J. A. White, Int. J. Thermophys. **22,** 1147 (2001).
[17] S. B. Kiselev and J. F. Ely, Fluid Phase Equilib. **222–223,** 149 (2004).
[18] L. Kudelkova, J. Lovland, and P. Vonka, Fluid Phase Equilib. **218,** 103 (2002).
[19] S. B. Kiselev and J. F. Ely, Ind. Eng. Chem. Res. **38,** 4993 (1999).
[20] S. B. Kiselev, J. F. Ely, H. Adidharma, and M. Radosz, Fluid. Phase. Equilib. **183–184,** 53 (2000).
[21] S. B. Kiselev and J. F. Ely, Fluid Phase Equilib. **174,** 93 (2000).
[22] S. B. Kiselev, J. F. Ely, I. M. Abdulagatov, and J. W. Magee, Int. J. Thermophys. **6,** 1373 (2000).
[23] C. McCabe and S. B. Kiselev, Ind. Eng. Chem. Res. **43,** 2839 (2004).
[24] Z.-Q. Hu, J.-C. Yang, and Y.-G. Li, Fluid Phase Equilib. **205,** 1 (2003).
[25] Z.-Q. Hu, J.-C. Yang, and Y.-G. Li, Fluid Phase Equilib. **205,** 25 (2003).
[26] M. A. Anisimov, *Critical Phenomena in Liquids and Liquid Crystals* (Gordon and Breach, New York, 1991).
[27] S. B. Kiselev, J. F. Ely, Chem. Eng. Sci. **61**, 5107 (2005).
[28] P. Schofield, Phys. Rev. Lett. **22,** 608 (1969).
[29] B. D. Josephson, J. Phys. C **2,** 1113 (1969).
[30] S. B. Kiselev and J. F. Ely, J. Chem. Phys. **119,** 8645 (2003).
[31] J. R. Elliott Jr and L. Hu, J. Chem. Phys. **110,** 3043 (1999).
[32] E. d. Miguel, Phys. Rev. E **55,** 1347 (1997).
[33] G. Orkoulas and A. Z. Panagiotopoulos, J. Chem. Phys. **110,** 1581 (1999).
[34] S. B. Kiselev and J. F. Ely, J. Chem. Phys. **120,** 8241 (2004).
[35] J. K. Singh, D. A. Kofke, and J. R. Errington, J. Chem. Phys. **119,** 3405 (2003).
[36] D. A. Young, J. Chem. Phys. **58,** 1647 (1973).
[37] D. A. Young and B. J. Alder, J. Chem. Phys. **73,** 2430 (1980).
[38] J. R. Elliott and L. Hu, J. Chem. Phys. **110,** 3043 (1999).
[39] M. H. J. Hagen and D. Frenkel, J. Chem. Phys. **101,** 4093 (1994).
[40] B. Chen, J. I. Siepmann, S. Karaborni, and M. L. Klein, J. Phys. Chem. B **107,** 12320 (2003).
[41] J.-J. Weis, Mol. Phys. **28,** 187 (1974).
[42] J. J. Weis, Mol. Phys. **32,** 296 (1976).
[43] H. S. Kang, T. Ree, and F. H. Ree, J. Chem. Phys. **84,** 4547 (1986).
[44] L. Vega, E. de Miguel, and L. F. Rull, J. Chem. Phys. **96,** 2296 (1992).
[45] E. de Miguel, Phys. Rev. E **55,** 1347 (1997).
[46] F. del Rio, E. Avalos, R. Espindola, L. F. Rull, G. Jackson, and S. Lago, Mol. Phys. **100,** 2531 (2002).
[47] Release of the IAPWS *Formulation 1995 for the Thermodynamic Properties of Ordinary Water Substance for General and Scientific Use*, Frederica, Denmark (1996).
[48] N. B. Vargaftik, *Handbook of Physical Properties of Liquids and Gases* (Hemisphere Publishing Co., Washington, 1983).